Intra- and paraorbital lesions: value of fat-suppression MR imaging with paramagnetic contrast enhancement.

R D Tien, P K Chu, J R Hesselink and J Szumowski

AJNR Am J Neuroradiol 1991, 12 (2) 245-253
http://www.ajnr.org/content/12/2/245

Intra- and Paraorbital Lesions:
Value of Fat-Suppression MR Imaging with Paramagnetic Contrast Enhancement

Robert D. Tien[1]
Pauline K. Chu[1]
John R. Hesselink[1]
Jerzy Szumowski[2]

The orbital area of 18 individuals was examined by using a combination of fat-suppression contrast-enhanced MR imaging to determine whether contrast between fat and surrounding tissues could be improved over that obtained with conventional fat-suppression techniques alone. We used a hybrid technique combining two independent methods of fat suppression. Subjects consisted of 16 patients and two normal volunteers. Fifteen individuals received gadopentetate dimeglumine, and conventional T1-weighted, T2-weighted, and fat-suppression T1-weighted images were obtained. The fat-suppressed T1-weighted images obtained after contrast administration provided more information than did the conventional MR images. Intraorbital and paraorbital lesions could be distinguished easily from intraorbital fat that had been suppressed. Cases of chorioretinitis and optic neuritis could be confidently diagnosed only by this technique. Cases of optic nerve meningioma and mixed conal lesions also were better appreciated. Because of sharp contrast between tissue planes, this technique was helpful for detecting any intraorbital invasion from paraorbital lesions.

Fat-suppression MR imaging with paramagnetic contrast enhancement can significantly improve the delineation of both normal and abnormal structures and better define lesional margins in the orbit, where large amounts of fat are present. Our results support earlier findings, and we suggest that postcontrast fat-suppressed T1-weighted imaging be used instead of conventional T1-weighted postcontrast imaging in evaluating orbital and paraorbital lesions.

***AJNR* 12:245–253, March/April 1991; *AJR* 156: May 1991**

In regions of high fat content, such as the orbit, anatomic details are not optimally appreciated on conventional MR images. Although contrast enhancement can improve the ability to distinguish between a lesion and surrounding structures, distinction between enhanced structures and fatty tissue remains difficult in areas with significant amounts of fat. Various fat-suppression techniques have been devised that significantly improve the depiction of anatomic details [1]. In addition, in a preliminary study, the administration of a paramagnetic contrast agent, gadopentetate dimeglumine, in combination with a modified chopper fat-suppression technique was found to be the best way to depict lesions located in areas with large amounts of fat [2]. We applied this technique, focusing on orbital lesions, to determine if these structures would similarly reveal significantly improved anatomic detail.

Materials and Methods

MR imaging of the orbit was performed in 16 consecutive patients and two volunteers (12 males, six females), ranging in age from 5 months to 72 years (average, 32 years). Fifteen subjects received gadopentetate dimeglumine (Magnevist; Berlex, Cedar Knolls, NJ). The pathologic diagnoses are given in Table 1.

All MR studies were performed on a 1.5-T unit (Signa; General Electric, Milwaukee, WI) with a quadrature head coil. The studies included a conventional unenhanced T1-weighted

Received May 8, 1990; revision requested July 2, 1990; revision received October 4, 1990; accepted October 10, 1990.

[1] Department of Radiology and the Magnetic Resonance Institute, UCSD Medical Center, 225 Dickinson St., San Diego, CA 92103. Address reprint requests to R. D. Tien.

[2] Department of Radiology, Oregon Health Sciences University, Portland, OR 97201.

0195–6108/91/1202–0245

TABLE 1: Composition of the Study Group (n = 18)

Diagnosis	No.
Normal	3
Global lesions	
Cytomegalovirus chorioretinitis	1
Chorioretinitis	1
Choroidal melanoma	1
Intraconal lesions	
Optic neuritis	1
Optic meningioma	1
Muscle cone lesion	
Graves disease	1
Extraconal lesions	
Plexiform neurofibroma	1
Epibulbar dermoid	1
Dacryocystocele	1
Mixed intra- and extraconal lesions	
Plexiform neurofibroma	2
Adenoid cystic carcinoma	1
Lesions adjacent to the orbit	
Sphenoid meningioma	1
Adenoid cystic carcinoma of the maxillary sinus	1
Polyposis of the ethmoid sinus	1

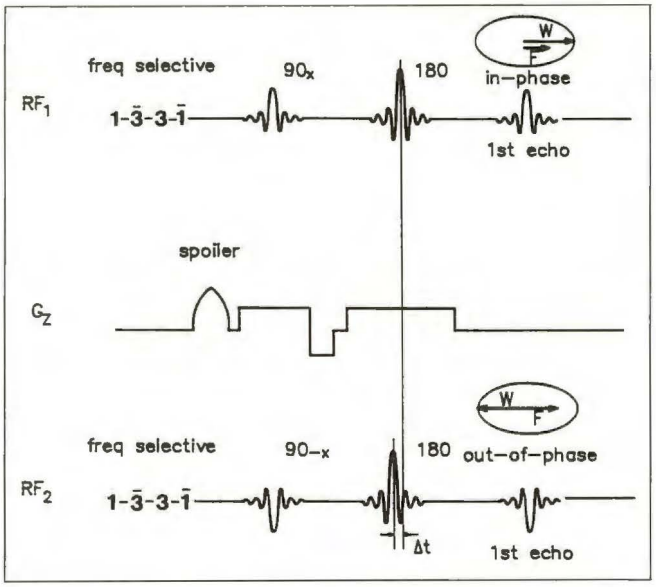

Fig. 1.—Diagram of hybrid pulse sequence used in this study. A frequency-selective pulse centered on fat resonance (in this case the 1331 pulse described by Hore [8]) is followed by chopper fat signal elimination. Two independent mechanisms of fat suppression applied together in one sequence substantially improve the effectiveness of fat/water signal separation.

spin-echo series, 600/20 (TR/TE), in 15 patients; proton-density and T2-weighted imaging, 3000/30,80, in 14 patients; and a T1-weighted fat-suppression image in all patients. In addition, contrast-enhanced T1-weighted images were obtained in eight patients.

We used a hybrid technique of fat suppression in the spin-echo mode of data acquisition. The technique incorporates two independent physical mechanisms for lipid signal elimination. The advantages of the frequency-selective excitation method and chopper [3–6] phase-sensitive variant of the Dixon method [7] were combined into a single two-excitation sequence.

A diagram of the hybrid sequence is presented in Figure 1, in which our implementation, a so-called 1331 frequency-selective pulse [8] was incorporated with an in- and out-of-phase data collection. The effect of pulse sequence on the fat and water magnetization vectors is represented in detail in Figure 2. The resulting water-only image is characterized by a more uniform fat signal suppression and a better suppression factor than if either method was used independently. The performance of the hybrid sequence has been tested on phantoms and volunteers, and the results have been presented in a separate study [3]. This technique achieves high-level lipid suppression without increasing imaging time or image postprocessing. The technique requires B_0 field homogeneity over the field of view exceeding the chemical shift difference between lipid and water. With this condition, the hybrid method has been applied with a high-field-strength magnet; however, it might be used with a mid-field-strength magnet if the field homogeneity permits.

Images were obtained in the coronal or axial plane, or both. Other imaging parameters included a 16-cm field of view, 3-mm slice thickness with 1-mm interslice gap, a 256 × 192 matrix, and 1–4 excitations. The resultant conventional images and paired fat-suppression images were carefully compared for demonstration of normal anatomic detail, increased conspicuity of enhancing lesions, delineation of lesional margins, and existence of an interface between lesions and normal structures.

Results

The pathologic diagnoses are listed in Table 1.

Normal Subjects

The precontrast T1-weighted hybrid images showed the reversal of normal T1 contrast, with ratios of the signal intensity strongly positive between the optic nerve and fat, lacrimal gland and fat, and extraocular muscle and fat. The thicknesses of the optic nerve, muscle contour, and lacrimal gland were clearly represented (Fig. 3). Intracanalicular optic nerves were clearly seen when surrounding intracanalicular fat and fatty marrow signal were eliminated (Fig. 4). After contrast administration, the muscles and lacrimal gland enhanced intensely. However, the optic nerve did not enhance (Fig. 3H). The conventional long TR/long TE images did not suppress the intraorbital fat signal satisfactorily in all patients in our study. Compared with conventional spin-echo images (either T1- or T2-weighted), the postcontrast hybrid T1-weighted images gave the best normal anatomic definition between intraorbital structures. There was a magnetic susceptibility artifact on hybrid images between the sinuses and frontal lobes along the frequency-encoding axis due to air and soft-tissue interface (Figs. 3F and 3I). In our limited experience (to date, about 30 patients), the artifact was usually small, was found mainly in the frontal lobes, and did not interfere with the clear visualization of the orbit.

Global Lesions

Strong and distinct, irregular enhancement of the posterior chorioretina was clearly noted on axial postcontrast hybrid T1-weighted images in two patients with acute blindness (Fig. 5). One patient had conventional postcontrast T1-weighted imaging in the coronal plane but this was unremarkable (Fig.

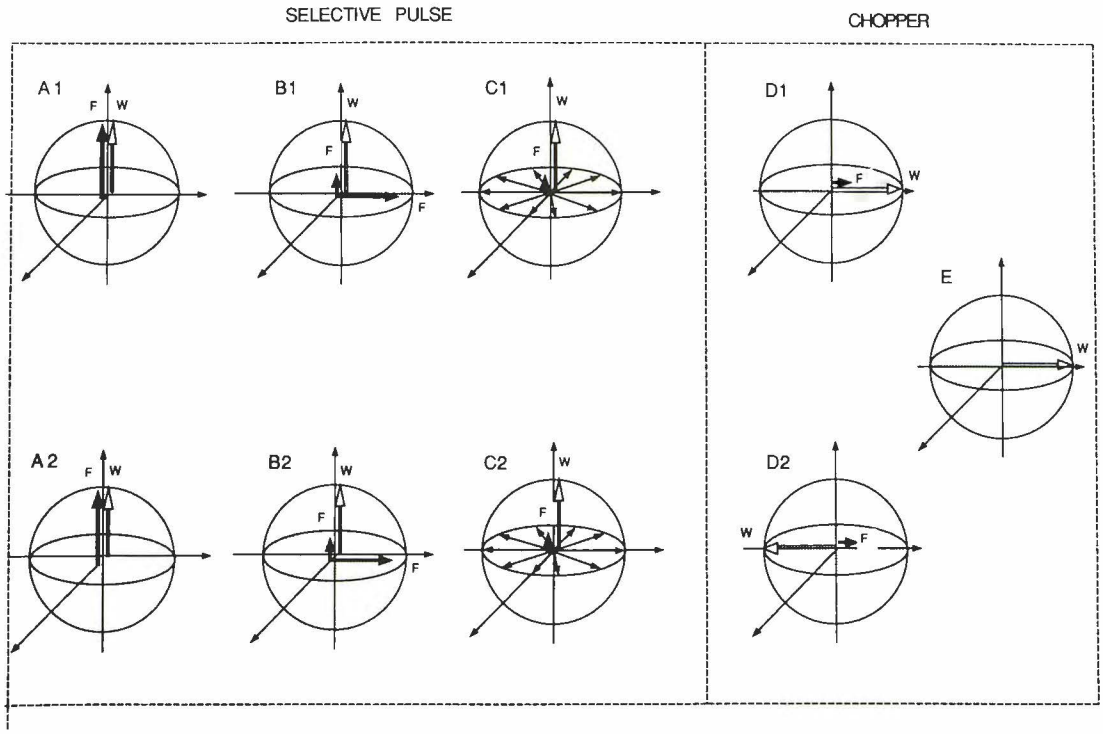

Fig. 2.—Graphic representation of magnetic behavior in the hybrid pulse sequence as applied to lipid signal suppression with the frequency of the MR scanner tuned to water resonance and the frequency-selective pulse centered on fat resonance.

During the first excitation (A1) the lipid magnetization is rotated into the transverse plane (B1) and dephased by the spoiler gradient (C1). This frequency-selective pulse provides partial elimination of the lipid signal subject to the limitations of magnetic field B_0 and RF inhomogeneities. The rest of the sequence operates on the remaining lipid and water magnetizations to produce the in-phase echo (D1).

During the second excitation, the frequency-selective pulse and dephasing gradients are repeated (A2, B2, C2); however, the phase of the slice-selective pulse is reversed and the timing of the refocusing pulse is adjusted to produce the out-of-phase echo (D2). Averaging by subtraction during the data acquisition, as in the original chopper fat-suppression sequence, results in elimination of the remnant lipid component in the final image (E).

5C). Chorioretinitis was diagnosed (one patient had cytomegalovirus infection, one had retinal biopsy, which revealed herpesvirus infection). These findings were unidentifiable on conventional proton-density and T2-weighted images (Figs. 5D and 5E).

One patient had presumed choroidal melanoma diagnosed by sonography. Despite being told that the chances of success with iodine-125 plaque implantation were minimal because his tumor was so large, the patient chose the plaque implant instead of enucleation. Although we did not obtain tissue in this case, the diagnostic accuracy was believed to be very high. The postcontrast hybrid T1-weighted image clearly showed the inhomogeneously enhancing posterior global mass. The tumor could be seen on conventional proton-density images but not as well, and it could not be identified at all on conventional T2-weighted images (Fig. 6).

Intraconal Lesions

In the patient with right optic neuritis resulting from CNS sarcoidosis, conventional T1- (Fig. 7A) and T2-weighted images failed to show any size or signal abnormalities of the optic nerves. The postcontrast T1-weighted image (Fig. 7B) showed mild enhancement of the upper portion of the posterior right optic nerve. However, the postcontrast hybrid T1-weighted image (Fig. 7C) clearly demonstrated the strong enhancement (to the same degree as muscle) of the right optic nerve over its entire cross section from the retrobulbar portion to the intracanalicular portion, suggesting the inflammatory nature of the disease.

In another patient with suspected left optic nerve meningioma (Fig. 8), the bumpy mass was demonstrated by conventional T1-weighted imaging (before and after contrast administration) and by precontrast hybrid T1-weighted imaging. However, the linear low signal interface between the tumor and optic nerve (so-called tram-track sign, characteristic of the optic nerve meningioma) could be easily identified on the postcontrast hybrid T1-weighted image.

Muscle Cone Lesion

In one woman with clinical hyperthyroidism and mild right exophthalmos, MR was requested to rule out Graves disease. On conventional T1-weighted images, slightly thickened right inferior and perhaps medial rectus muscles were noted (Fig. 9A). On postcontrast T1-weighted fat-suppression images, the thickened right inferior and medial rectus muscles, as well as surrounding inflammatory infiltrate, were imaged clearly (Fig. 9B).

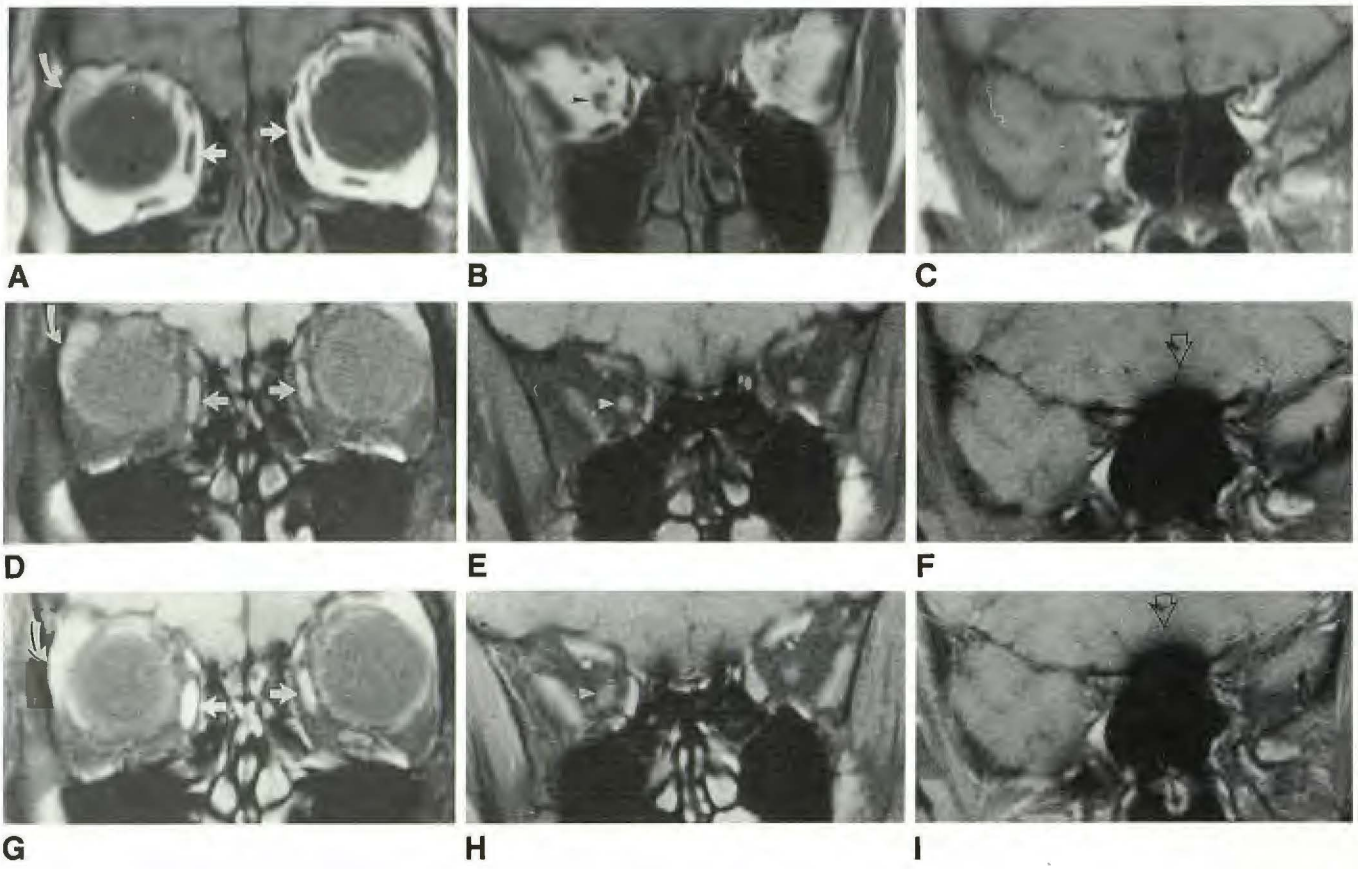

Fig. 3.—Normal volunteer. Coronal T1-weighted images (600/20/2) (*A–C*), coronal T1-weighted images with fat suppression (*D–F*), and postcontrast coronal T1-weighted images with fat suppression (*G–I*). Margins and outlines of extraocular muscles (*straight white arrows*), optic nerves (*arrowheads*), and lacrimal glands (*curved arrows*) are much better defined on fat-suppression images. Extraocular muscles enhance intensely and they appear slightly larger than on conventional T1-weighted images. Also, there is increased magnetic susceptibility artifact at ethmoid air cells and subfrontal regions on the fat-suppression images (*open black arrows*); however, the orbits are not affected significantly.

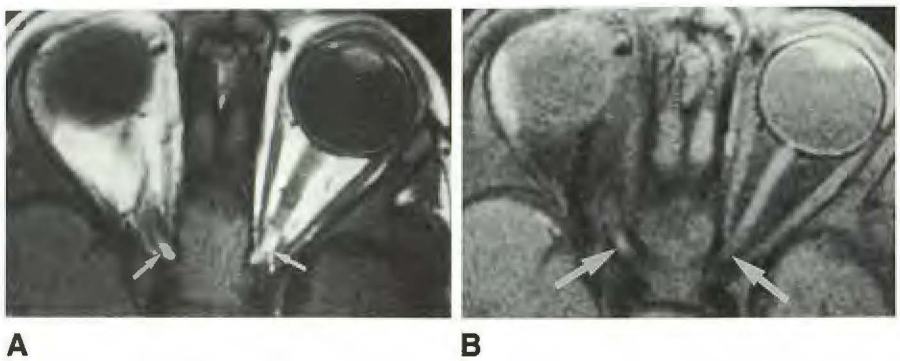

Fig. 4.—Normal volunteer.
***A*, Axial T1-weighted image (600/20/2). Intracanalicular portion of optic nerves was obscured by high-signal fat (*arrows*).**
***B*, Axial T1-weighted image with fat suppression. Intracanalicular portion of optic nerves (*arrows*) is seen much better on fat-suppression image.**

Extraconal Lesions

One young patient with neurofibromatosis and an orbital mass identified on CT scan was studied. The postcontrast hybrid T1-weighted image clearly showed the enhancing wormlike mass and its extraconal location, but its entire extent could not be clearly identified on conventional MR images.

An infant with clinically diagnosed Goldenhar syndrome was studied to rule out any brain abnormality. A small left epibulbar mass of high signal intensity was noted on T1-weighted images (Figs. 10A and 10B). Hybrid T1-weighted imaging successfully suppressed the high signal portion of the mass, proving it to be a fatty mass (Fig. 10C) and confirming the diagnosis of epibulbar dermoid, which is one of the associated congenital abnormalities in Goldenhar syndrome.

One infant with a left-sided lower eyelid mass was studied. Conventional MR images showed a well-defined oval mass in the left medial canthus that was of low signal intensity on T1-weighted images and of high intensity on T2-weighted images. The hybrid T1-weighted images showed the mass to

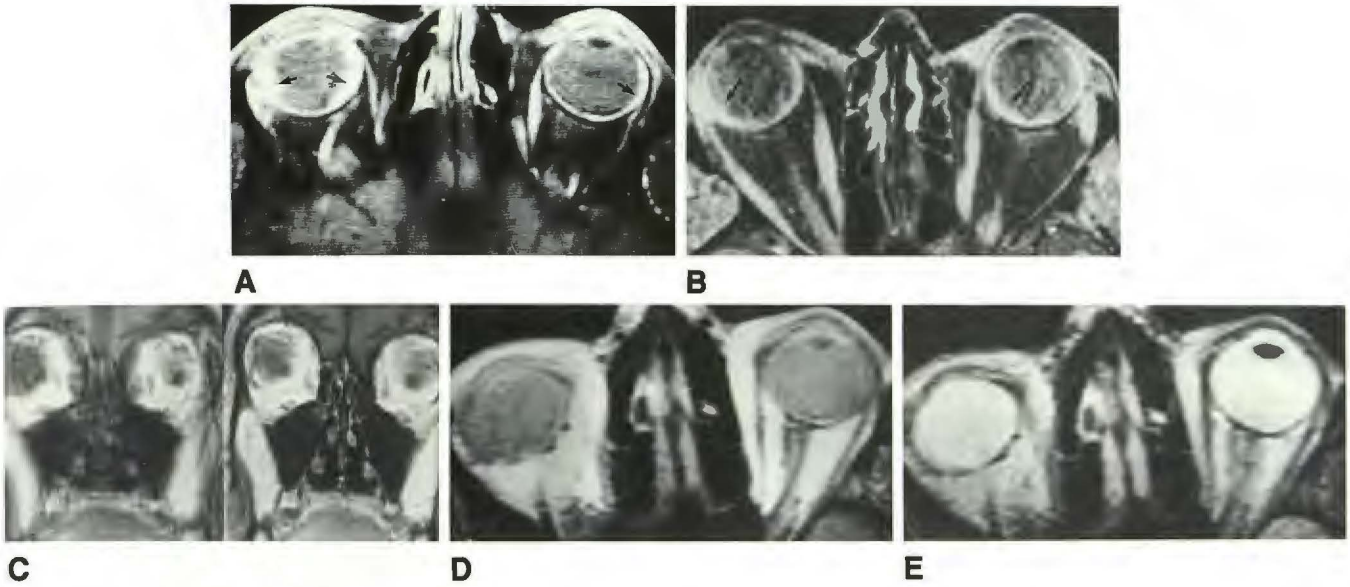

Fig. 5.—Two patients with acute vision loss.
A and *B*, Postcontrast axial T1-weighted images (600/20/2) with fat suppression in patients 1 (*A*) and 2 (*B*) show bilateral abnormal, irregularly thickened and enhanced chorioretina (*arrows*).
C–E, Conventional spin-echo images of patient 1 are unremarkable: postcontrast T1-weighted image (600/20/2) (*C*), proton-density image (*D*), and T2-weighted image (2000/20,80/2) (*E*). The diagnosis of chorioretinitis was established clinically.

Fig. 6.—60-year-old man with choroidal melanoma diagnosed by sonography.
A, Proton-density image (2000/30/2) shows a lenticular-shaped mass in left lateral globe (*arrows*).
B, T2-weighted image (2000/80/2) is unremarkable.
C, Postcontrast fat-suppression image (600/20/2) clearly shows the mass. The right extension of mass (*arrows*) is seen better here than on proton-density image.

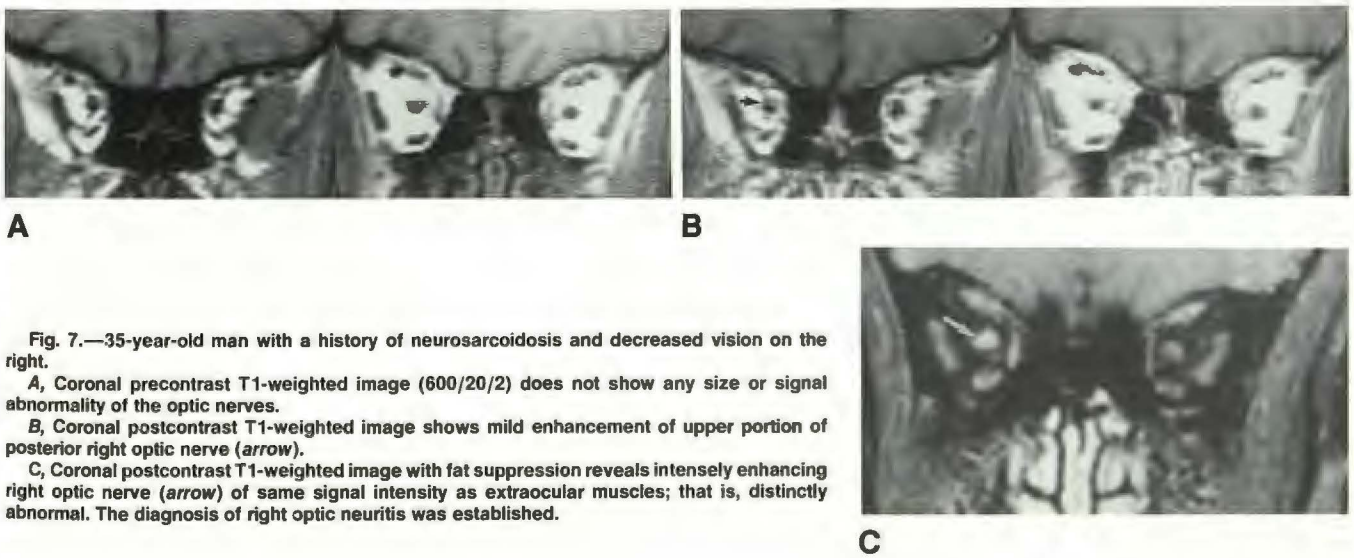

Fig. 7.—35-year-old man with a history of neurosarcoidosis and decreased vision on the right.
A, Coronal precontrast T1-weighted image (600/20/2) does not show any size or signal abnormality of the optic nerves.
B, Coronal postcontrast T1-weighted image shows mild enhancement of upper portion of posterior right optic nerve (*arrow*).
C, Coronal postcontrast T1-weighted image with fat suppression reveals intensely enhancing right optic nerve (*arrow*) of same signal intensity as extraocular muscles; that is, distinctly abnormal. The diagnosis of right optic neuritis was established.

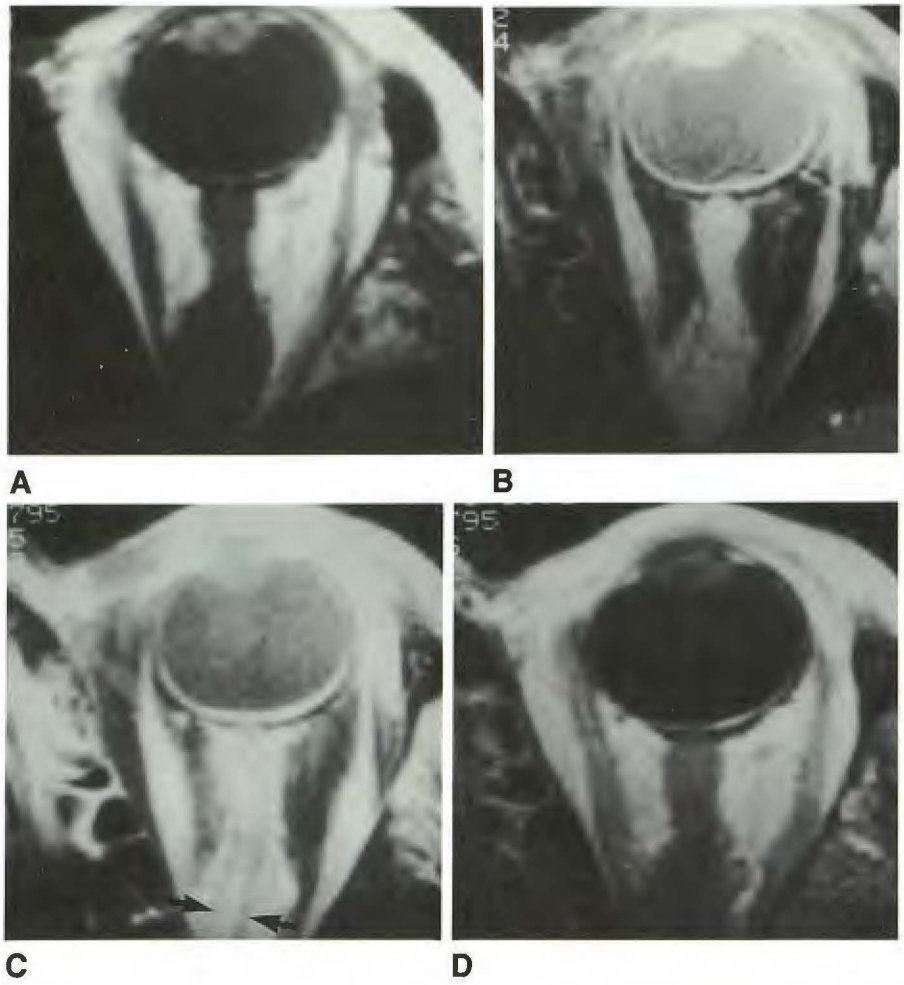

Fig. 8.—60-year-old woman with left visual loss.

A–D, Axial T1-weighted image (600/20/2) (*A*), T1-weighted image with fat suppression (*B*), postcontrast T1-weighted image with fat suppression (*C*), and postcontrast T1-weighted image without fat suppression (*D*) all show bumpy perineural tumor. In *C*, the tram-track sign (*arrows*) is clearly visible, which is typical of optic nerve meningioma.

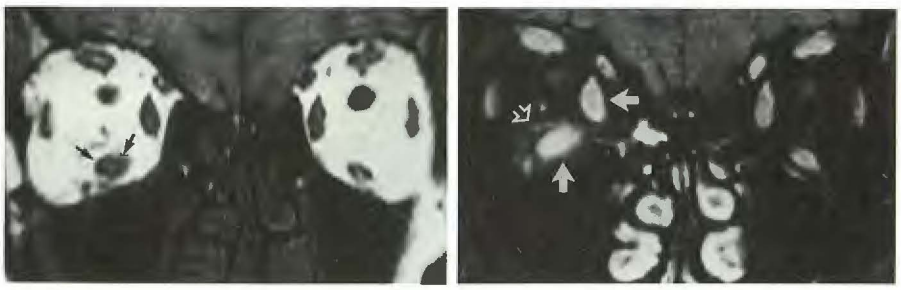

Fig. 9.—33-year-old woman with hyperthyroidism and mild right exophthalmos.

A, Coronal T1-weighted image (600/20) shows mild thickening of right inferior rectus muscle (*arrows*) and perhaps of right medial rectus muscle.

B, Postcontrast coronal T1-weighted image (600/20) clearly shows the thickened and intensely enhancing right inferior and medial rectus muscles (*solid arrows*) as compared with left eye. Inflammatory infiltrate around right inferior rectus muscle is also noted (*open arrow*).

Fig. 10.—5-month-old boy with clinical probability of Goldenhar syndrome.

A and *B,* Axial (*A*) and coronal (*B*) T1-weighted images (600/20/2) reveal high-signal tissue in left epibulbar space (*arrows*) just inferior to lacrimal gland.

C, Coronal T1-weighted image (600/20/1) with fat suppression completely suppresses the signal from this tissue (*arrow*), thus indicating its fatty nature. This tissue is consistent with an epibulbar dermoid, which is frequently seen in patients with Goldenhar syndrome. Because the baby was waking up from sedation, we performed the sequence by using 1 excitation and a 256 × 128 matrix to shorten the study time. Thus, these images have a low signal-to-noise ratio.

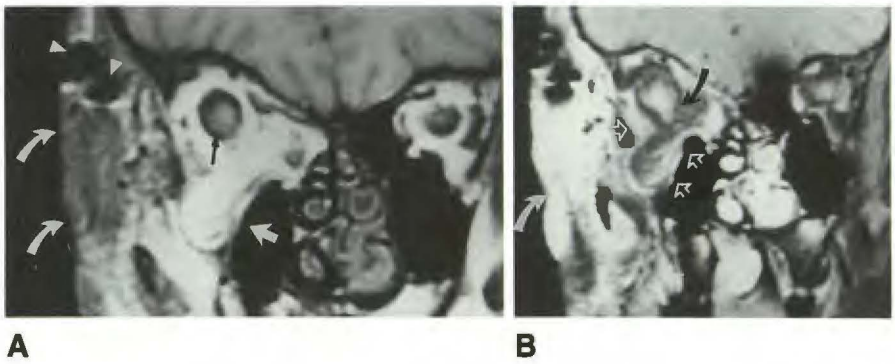

Fig. 11.—20-year-old man with neurofibromatosis.

A, **Coronal T1-weighted image (600/20/2) reveals a dysplastic right bony orbit. High-signal intraorbital fat appears to herniate into upper maxillary sinus (*straight white arrow*). Also, abnormal soft tissue in right face (*curved white arrows*) and large optic nerve (*black arrow*) are noted. Some metallic susceptibility artifacts were seen in right temporal region (*arrowheads*), induced by clips from a prior biopsy.**

B, **Coronal postcontrast T1-weighted image (600/20/2) with fat suppression shows the enhancing plexiform neurofibromas involving the optic nerve (*curved black arrow*), muscle cone (*open white arrows*), and right facial muscles (*curved white arrow*). Margins of tumors can be seen much better.**

Fig. 12.—35-year-old man with a history of adenoid cystic carcinoma of the right submandibular gland.

A, **Coronal T1-weighted image (600/20/2) shows right orbit filled with tumor. A small hypointense artifact from radioactive material implant is noted (*arrow*).**

B, **Axial postcontrast T1-weighted image shows enhancing tumor in right orbit and its large intracranial component. Leptomeningeal spread (*white arrows*) and sphenoid infiltration (*black arrow*) are evident.**

C, Postcontrast T1-weighted image with fat suppression clearly shows both the inferior and lateral margins of tumor (*large black arrows*) and leptomeningeal tumoral extension (*small black arrow*).

be hyperintense relative to surrounding suppressed fatty tissue, and the margins of the mass were depicted better than on conventional MR images. This was proved to be a dacryocystocele.

Mixed Intra- and Extraconal Lesions

The postcontrast hybrid T1-weighted images were superior for detecting the enhancing tumors and for depicting the lesion margins in three patients with intraorbital masses—two plexiform neurofibromas (Fig. 11) and one adenoid cystic carcinoma (Fig. 12).

Lesions Adjacent to the Orbit

One patient with left sphenoid ridge meningioma was studied to evaluate the possibility of invasion of the lesion into the optic canal. The postcontrast hybrid T1-weighted images clearly demonstrated the enhancing sphenoid meningioma and showed the intracanalicular optic nerve to be intact.

Two other patients had soft-tissue masses in the sinuses with possible intraorbital invasion. One had adenoid cystic carcinoma of the left maxillary sinus, with the tumor attached to the floor of the orbit, and another patient had ethmoidal masses that proved to be polyposis (Fig. 13). In each case, the postcontrast hybrid coronal T1-weighted images demonstrated sharper tissue margin contrast between the enhanced mass and the intraorbital contents than did the conventional MR images.

Discussion

Large amounts of fat in the orbit outline the optic nerve sheath and extraocular muscle sheaths, globe, and orbital vessels. High contrast/noise ratios are obtained on T1-weighted images for most anatomic structures except the lacrimal gland. However, the high-intensity bands perpendicular to the frequency-encoding axis at the fat-water interface from chemical-shift misregistration can be seen parallel to the long axis of the optic nerve sheath and muscles on the axial images, and above and below the nerve and muscles on the coronal images, in accordance with the direction of the frequency-encoding gradient, which obscures the details of the optic nerve and extraocular muscles ([1] and Quencer et al., paper presented at the annual meeting of the Radiological Society of North America, Chicago, December 1988). Also, the intracanalicular segment of the optic nerve is often obscured by marrow signal from the adjacent bony canal, and

Fig. 13.—17-year-old boy with biopsy-proved ethmoidal polyposis.
***A* and *B*, Conventional coronal T1-weighted image (600/20/2) (*A*) and conventional coronal T2-weighted image (2000/70/2) (*B*) show diffuse soft tissue in ethmoidal and frontal sinuses. However, the orbital and polypoid tissue interface is not entirely distinct (*white arrows* in *A*, *black arrow* in *B*).**
***C*, Postcontrast T1-weighted image (600/20/2) with fat suppression sharply delineates entire tissue interface (*arrowheads*). There is no evidence of intraorbital invasion by this soft tissue.**

the high-signal orbital fat interfaces with the separation of the optic nerve, CSF, and dural sheath. The posterior wall of the globe contrasts poorly with adjacent vitreous humor.

With current fat-suppression techniques, the signal intensity relationships between the optic nerve and fat, lacrimal gland and fat, and muscle and fat reversal to strongly positive ratios, resulting in a more accurate representation of the thickness of the optic nerve, muscles, and contour of the lacrimal gland [4] (Fig. 3). The elimination of chemical-shift artifact results in truer anatomic borders. The intracanalicular optic nerve is more clearly identified owing to removal of the surrounding fatty marrow signal (Fig. 4). After contrast administration, the extraocular muscles and lacrimal glands enhance intensely but the optic nerves do not enhance (Fig. 3H). As a result, the margins of these structures are seen even better than with noncontrast fat-suppression T1-weighted imaging. The posterior wall of the globe also enhances as a thin, smooth line of high signal intensity, probably from the combined enhancement of vasculature structures in the chorioretina, the uveal-scleral coat, and the posterior fascial sheath of the eye (Tenon capsule). Although we used a combination of the frequency-selective excitation method and the chopper variant of Dixon's method, other methods of fat suppression can be used provided that fat is suppressed uniformly [8, 9]. For example, it has been demonstrated that the gradient reversal technique has been applied successfully to eliminate lipid signal in the orbits [8]. However, the use of STIR (short T1 inversion recovery) sequences might be suboptimal in conjunction with the paramagnetic contrast agent because while the STIR sequence eliminates the fat signal, it also decreases the signal of the lesion—a phenomenon known as negative enhancement [10].

The two cases of chorioretinitis (Fig. 5) were only detected on postcontrast fat-suppressed T1-weighted images as irregularly thickened enhancing bands that were distinctly different from normal enhancing tissue. In the case of choroidal melanoma, the postcontrast fat-suppressed T1-weighted image gave the best definition of the tumor. It was also seen well on noncontrast proton-density images, but was totally isointense with vitreous on T2-weighted images. Because of the sharp contrast between the vitreous posterior wall of the globe and suppressed adjacent intraorbital fat, we believe postcontrast fat-suppressed T1-weighted imaging will give the best definition of the margins of an enhancing global tumor. In the case of optic neuritis, the involved optic nerve enhanced to a similar degree as the extraocular muscles, and was distinctly abnormal on postcontrast fat-suppressed T1-weighted images (Fig. 7C). The diagnosis could not be made confidently on any other MR sequences. In a general article reviewing fat-suppression imaging with contrast-enhanced imaging [5], the authors stated that while they had limited experience with this technique in acute optic neuritis, enhancement might be expected in the acute demyelinating-inflammatory stage. Our preliminary, limited experience concurs with that postulate.

The tram-track sign, typical of optic meningioma, was only seen with certainty on postcontrast fat-suppression T1-weighted imaging because of better tissue contrast between the tumor and perineural subarachnoid space (Fig. 8). Owing to large amounts of intraorbital fat, tumor invasion into the orbit is always a problem for conventional MR. The high-signal orbital fat frequently obscures the margins of tumor, and volume-averaging artifact from fat always causes difficulty in noncontrast T1-weighted imaging. After contrast administration, the enhancing tumor blends with the orbital fat and further degrades the images. We found that postcontrast fat-suppression T1-weighted imaging gave superior contrast for detecting enhancing tumor and its margins in any intraorbital compartment. Inflammatory infiltration of the paramuscular fat in Graves disease could only be seen on postcontrast T1-weighted fat-suppression images (Fig. 9). Dermoid is also a common lesion in the area of the lacrimal fossa. A single fat-suppression T1-weighted image can easily provide the diagnosis (Fig. 10). The conventional long TR/long TE images did not suppress intraorbital fat signal satisfactorily, and chemical-shift artifact was still noticed in our patients. We found these

sequences were not very useful in diagnosing orbital lesions. Owing to the insensitivity of conventional MR imaging for detecting bony cortex and the possibility of a lesion being obscured by interference from the high-signal intraorbital fat, CT is still frequently requested to assess the possibility of intraorbital invasion by tumor or infection from adjacent compartments, such as maxillary sinuses, ethmoidal sinuses, and sphenoid ridge. However, the sharp contrast between enhancing masses relative to the suppressed intraorbital fat on postcontrast fat-suppressed T1-weighted images may be useful in evaluating intraorbital extension of a lesion, although the integrity of the bone itself is still difficult to assess (Fig. 13). The specific reason that the lesion margins were displayed better on the hybrid, contrast-enhanced image in the patient with ethmoidal polyposis is not entirely clear; however, the most likely explanation is that the inflammatory process in the ethmoidal sinuses induced secondary edema in the adjacent orbital fat. With contrast administration plus fat suppression, the enhancing polyps and inflammatory membranes within the sinuses are contrasted against the nonenhancing edema.

In conclusion, although we found the hybrid technique promising, we need to emphasize that these preliminary results are based on a limited number of patients. We believe this fat-suppression technique has benefits and that it can be performed without increasing imaging time and image postprocessing. Uneven fat suppression can happen with a large field of view as a result of field inhomogeneity [5], although, to date, we have not noticed any uneven fat suppression in the orbits. We did, however, note a small increased magnetic susceptibility artifact between the ethmoid sinuses and frontal lobe due to air–soft tissue interface (Figs. 3F and 3I), but this artifact did not reduce our diagnostic accuracy. Conventional T1- and T2-weighted imaging might still be useful in certain cases of intraocular tumor, such as uveal melanotic melanoma, if enough melanin exists, since melanin can appear hyperintense on T1 images and hypointense on T2 images [11, 12]. The signal intensities on MR of our patient with choroidal melanoma did not help the diagnosis, probably owing to the low melanin content of the tumor [11].

Our preliminary data suggest that fat-suppression T1-weighted imaging is a useful adjunct in evaluating orbital and paraorbital lesions. Moreover, postcontrast fat-suppressed T1-weighted imaging is most beneficial and should replace conventional postcontrast T1-weighted imaging, as it provides the best anatomic details, improves the detection of the enhancing lesions, and defines tissue interfaces better without increasing imaging or postprocessing time.

ACKNOWLEDGMENT

We appreciate the editorial effort by Cathy Fix.

REFERENCES

1. Simon J, Szumowski J, Totterman S, et al. Fat-suppression MR imaging of the orbit. *AJNR* **1988**;9:961–968
2. Simon J, Szumowski J. Chemical shift imaging with paramagnetic contrast material enhancement for improved lesion depiction. *Radiology* **1989**;171:539–543
3. Szumowski J, Eisen JK, Vinitski S, et al. Hybrid methods of chemical-shift imaging. *Magn Reson Med* **1989**;9:379–388
4. Poon CS, Szumowski J, Plewes DB, et al. Fat/water quantitation and differential relaxation time measurement using chemical shift imaging technique. *Magn Reson Imaging* **1989**;7:369–382
5. Szumowski J, Plewes DB. Separation of lipid and water MR imaging signals by chopper averaging in the time domain. *Radiology* **1987**;165:247–250
6. Haase A, Frahm J, Hanicke W, et al. 1H NMR chemical shift selective (CHESS) imaging. *Phys Med Biol* **1985**;30:341–344
7. Dixon WT. Simple proton spectroscopic imaging. *Radiology* **1984**; 189–194
8. Hore PJ. Solvent suppression in Fourier transform NMR. *J Magn Reson* **1983**;55:283–291
9. Atlas SW, Grossman RI, Hackney DB, et al. STIR MR imaging of the orbit. *AJNR* **1988**;9:969–974
10. Bydder GM, Steiner RE, Blumgart LH, et al. MR imaging of the liver using short T1 inversion recovery sequences. *J Comput Assist Tomogr* **1985**;9:1084
11. Peyster RG, Augsburger JJ, Shields JA, et al. Intraocular tumors: evaluation with MR imaging. *Radiology* **1988**;168:773–779
12. Mafee MF, Peyman GA, Grisolano JE, et al. Malignant uveal melanoma and simulating lesions: MR imaging evaluation. *Radiology* **1986**;160: 773–780